Available online at www.sciencedirect.com
SCIENCE DIRECT®
Journal of Sound and Vibration 276 (2004) 781–806
JOURNAL OF SOUND AND VIBRATION
www.elsevier.com/locate/jsvi

Fault diagnosis of a vacuum cleaner motor by means of sound analysis

U. Benko[a,*], J. Petrovčič[a], Đ. Juričić[a], J. Tavčar[c], J. Rejec[c], A. Stefanovska[b]

[a] *Institute Jožef Stefan, Department of Systems and Control, Jamova 39, 1000 Ljubljana, Slovenia*
[b] *University of Ljubljana, Faculty of Electrical Engineering, Tržaška 25, 1000 Ljubljana, Slovenia*
[c] *Domel d.d., Otoki 21, 4228 Železniki, Slovenia*

Received 8 January 2003; accepted 5 August 2003

Abstract

Achieving high quality standards and 100% defect-free deliverables is becoming a trend among manufacturers of household appliances. In that respect, thorough and reliable end-tests represent an important step towards this goal. This paper deals with the design of end-test procedures for vacuum cleaner motors based on sound analysis. It is well known that sound carries important information about the condition of contact surfaces in rotating parts. The paper aims first to provide a thorough analysis of sound sources within the motor. Second, by using simple yet effective signal processing tools, it is shown that with sound analysis alone it is possible to clearly distinguish fault-free motors from those with mechanical faults. Moreover, the proposed algorithm exhibits a certain isolation capability, i.e., it is able to distinguish three clusters of faults. Finally, a summary of experimental results obtained on a sample of 75 motors is provided.

1. Introduction

Tough competition in the market between producers of household appliances has resulted in increasing demands for higher quality, (almost) 100% fault-free products, longer lifetimes and lower prices. In some sectors, e.g., washing machines and car manufacturing, standards are emerging that impose minimal requirements on the quality of delivered motors, for example vibration level and lifetime.

This appears to be an emerging trend in the vacuum cleaner manufacturing sector. The traditional process of quality assurance still relies partly on manual operations and subjective

*Corresponding author.
E-mail address: uros.benko@ijs.si (U. Benko).

0022-460X/$ - see front matter © 2003 Elsevier Ltd. All rights reserved.
doi:10.1016/j.jsv.2003.08.041

decisions, although some quality tests are well automated (e.g., rotor balancing or high voltage tests). However, in order to reduce the costs of the quality assurance process and to achieve entirely fault-free production, there is an emerging need for fully automated end-tests for each unit with more refined condition monitoring procedures.

The key part of a vacuum cleaner is the universal collector motor, a device widely used in almost all household appliances. The attribute "universal" indicates that such a motor can be connected to either an AC or DC voltage source. The key feature borrowed from classical DC motors is the use of brushes, while the structure of windings allows the application of AC voltage. These motors share similar moment characteristics with DC motors, which makes them attractive for use in commercial products.

The condition monitoring of collector motors and (in more general) rotating machines has been addressed by a number of authors; only a few will therefore be mentioned. For example, Yang and Penman [1] apply motor current and vibration sensing as a basis for feature extraction via artificial neural networks for bearing condition diagnosis. The same problem has been treated by Röpke and Filbert [2] via modern classification approaches, and by Filbert and Gühmann [3] via estimation of the current spectrum.

Feature extraction based on residuals generated through a mathematical model of electrical and mechanical parts has been addressed by, e.g., Filbert [4], Isermann [5], Vetter et al. [6] and Juričić et al. [7]. Vibrations appear as a valuable indicator of the condition of the rotating parts. Many papers address this issue, see Refs. [8,9] for an overview. Typically the authors combine vibration analysis with some of the advanced feature extraction methods. For example, Barkov and Barkova [10] applied an artificial intelligence approach for machine condition monitoring and diagnostics through vibration analysis, while Peng et al. [11] make use of the wavelet transform.

For industrial applications a proper combination of methods is required for the highest diagnostic resolution. Such an approach has been utilized by Vetter et al. [6], see also web page of Refs. [12,13].

The purpose of the paper is to investigate the potential of sound analysis in fault diagnosis of vacuum cleaner motors. It seems that very little attention has been paid to such a potentially relevant issue. Indeed, the sound produced by rotating parts is directly influenced by the condition of contact surfaces, the condition of bearings and deviations in the geometry of the aerodynamic parts. In the case of a vacuum cleaner, the fan impeller, which is mounted directly on the rotor shaft and represents the main sound source, is the key aerodynamic part. The goal of the authors is to design features based on sound signal analysis so that as much information as possible is obtained on fault location. Combined with features generated by other techniques (vibration analysis, residual generation based on a mathematical model, analysis of commutation), it is believed that a more accurate diagnostic system can be designed.

The experimental study has been conducted on 75 motors of which

- 15 were fault-free;
- 15 had improper brush–commutator contact;
- 15 had a bearing fault;
- 15 had contact between fan and housing;
- 15 had an unfamiliar noise (howling motors).

The paper is organized as follows. The experimental set-up is described in Section 2. Section 3 deals with the investigation of sound sources. In Section 4 the design of experiments and signal analysis tools is presented. Section 5 describes feature extraction in detail. Sections 6 and 7 deal with fault detection and fault localization of parts of the diagnostic procedure, respectively. Section 8 provides an excerpt from experimental results.

2. Experimental set-up

2.1. Vacuum cleaner motor

The central part of a vacuum cleaner is a universal collector motor with attached fan impeller. The fan is fixed on the shaft and rotates together with a rotor, thus giving the motor its primary function, i.e., air suction. Fig. 1 shows the most essential parts of the motor. The nominal operating conditions of the motor are as follows:

- applied AC voltage 230 V 50 Hz;
- 1.4 kW power;
- 38,000 r.p.m. (revolutions per minute);
- lifespan ca 700 h of operation.

2.2. Measuring equipment

In order to carry out experiments on the motors as well as to validate various fault diagnosis schemes, an experimental environment is built up around the echo-free sound chamber (see Fig. 2). The walls of this chamber are made of sound-absorbent material, which prevents sound reflection.

The *microphone* used has a frequency band of between 20 Hz and 20 kHz and a voltage/sound pressure sensitivity of 10 mV/Pa. The microphone is connected to the *amplifier,* which conditions

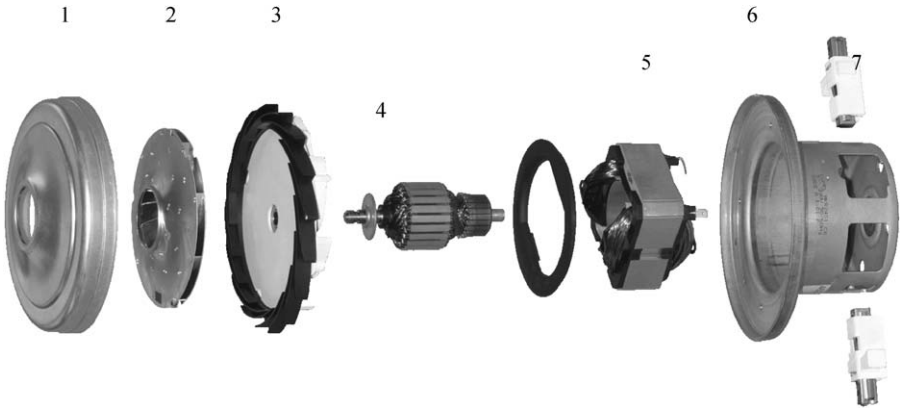

Fig. 1. Structure of a vacuum cleaner motor; turbine cover (1), fan impeller (2), diffuser (3), rotor (4), stator (5), motor housing (6) and brush (7).

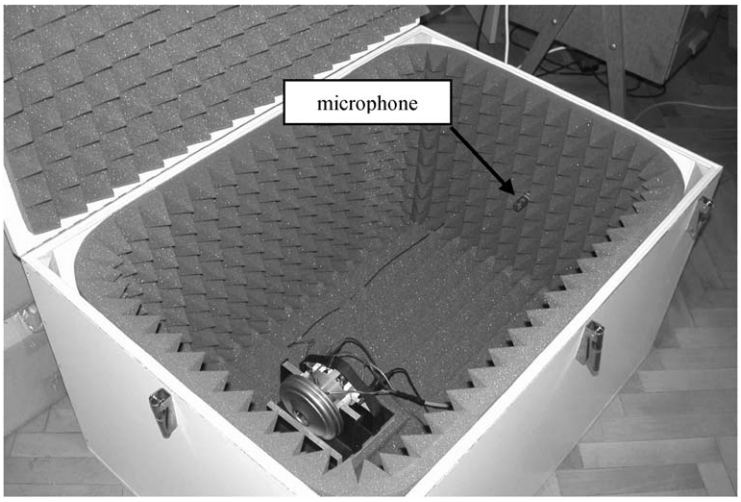

Fig. 2. Echo-free sound chamber.

the signal to the appropriate voltage level in the range ± 5 V. The microphone signal is passed through the anti-aliasing filter with a cut-off frequency of 13 kHz. An optical sensor attached to the motor is used to measure rotational speed.[1] Both signals are sampled at the frequency of 30 kHz.

3. Inventory of sound sources

The sound generated during rotation of the motor originates from three principal sources:

1. time-varying electromagnetic forces causing electromagnetic noise;
2. airflow aerodynamics and
3. mechanical contacts.

3.1. Electromagnetic noise

Electromagnetic noise appears only when AC voltage is applied to the motor. Indeed, time-varying voltage implies the variable magnetic flux of the stator, which in turn results in three phenomena:

- magnetostriction;
- electrostriction;
- time-varying rotor moment.

All these sources generate sound with a frequency twice that of the applied voltage frequency (similar to noise emitted by transformers).

[1] Actually, the experiments can be done without speed measurements. It was found out that rotational speed can be estimated from the sound signal itself using cepstrum analysis (see Ref. [14] for overview).

The dominant source is the time-varying rotor moment. It was found in experiments that the power of the corresponding noise is approximately 20 times higher than the power of the noise emitted by the remaining two sources. However, given the fact that the human ear has logarithmic characteristics, this ratio is perceived as being much lower, i.e., only twice as high. However, the three noise sources are caused by the nature of the supply voltage and, as such, carry almost no information on the condition of the motor. Consequently, they will be ignored in the following sections.

3.2. Aerodynamic noise

As the geometry of the motor is rather complex, the flow direction changes, thus causing turbulence. Other rotating parts (e.g., the rotor) also generate aerodynamic noise, but their contribution can be ignored. Experimental results show that aerodynamic sound intensity[2] strongly depends on rotational speed. The relationship between sound intensity and rotational speed can be approximated as

$$I \propto n^4, \tag{1}$$

where I denotes sound intensity and n denotes the rotational speed.

3.3. Mechanical noise

Vibrations of solid structures and mechanical contact between different surfaces of the motor components cause mechanical noise.

Vibrations arise from unbalanced rotating parts (i.e., fan impeller and rotor) and from forces caused by turbulent and variable airflow. These forces excite significant housing vibrations, especially at higher rotational speeds. The vibrational waves propagate all over the housing, thus creating reverberant vibrational fields that radiate sound.

Another source of mechanical noise is caused by mechanical contact and impact between two moving parts, in particular in bearings and in brush–commutator contact. Not only do both shorten the lifespan of the motor but also the sound coming out can be rather unpleasant for the user.

3.4. Relationships between various sound sources

During nominal operating conditions (38,000 r.p.m.), the noise of mechanical components is drowned out by aerodynamic noise. In fact, the experimental results show that this is the case for rotational speeds down to 2400 r.p.m. (research was done on a sample of 75 motors). Below this range the noise caused by mechanical contacts and other mechanical malfunctions becomes significant and, in a faulty motor, even prevalent compared to other sources. Namely, if the motor has a fault, the intensity of mechanical noise increases substantially in the lower range of rotational speeds and reaches much higher values (Fig. 4). Hence, this lower range of rotational speed seems to be the most appropriate for fault detection.

[2] Sound intensity refers to mean square sound pressure.

In addition, the intensity of mechanical noise changes according to rotational speed, depending on whether a motor is faulty or not. Fig. 3 shows the relationships between intensities of sound sources for rotational speeds below 3000 r.p.m. for a fault-free motor. Symbol n_1 denotes the rotational speed at which the noise of the fan becomes significant; it was estimated at 900 r.p.m. Symbol n_2 denotes the speed at which aerodynamics drown out the sound of the mechanical components; this boundary line is around 1800 r.p.m. Symbol n_3 is the upper limit of the rotational speed at which all sources are still detectable. The intensity of aerodynamic sound increases sharply after that limit and the other two sources become unrecognizable. The value of n_3 is between 2400 and 3000 r.p.m.

Fig. 4 depicts the relationships for a faulty motor. In this case, the landmark (n_3) moves toward higher values, even up to 4800 r.p.m.

Remark: The relationships presented in Figs. 3 and 4 are qualitative by nature and are based on experience obtained from experiments. Namely, most of the sound sources cannot be investigated separately one from another. The exception is electromagnetic noise which can partly be

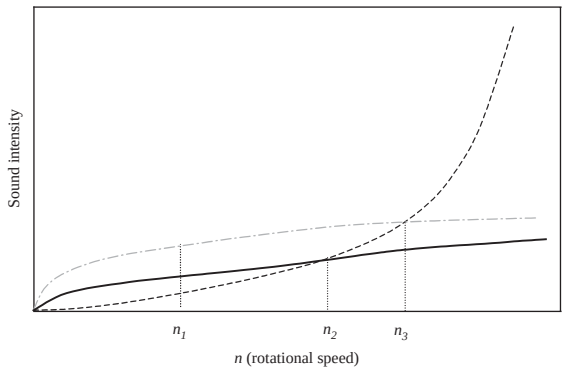

Fig. 3. Qualitative relationship between different sources of sound for a fault-free motor: mechanical components (solid line), aerodynamic components (dash line) and electromagnetic noise (dash–dot line).

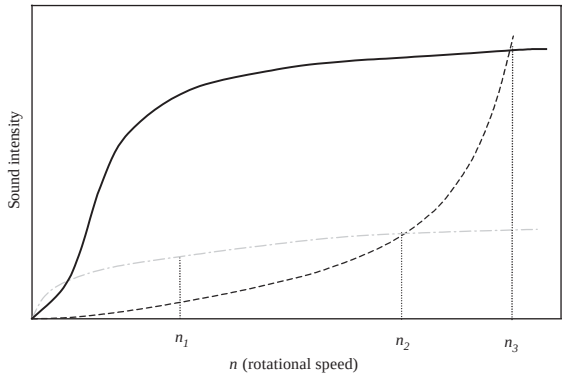

Fig. 4. Qualitative relationship between different sources of sound for a motor with a mechanical fault: mechanical components (solid line), aerodynamic components (dash line) and electromagnetic noise (dash–dot line).

quantified in the motor at standstill. To get the picture about other sources one has to analyze changes of characteristic frequencies in sound spectra recorded at different rotational speeds. That is why the characteristics in Figs. 3 and 4 cannot be exact but only qualitative.

4. Design of experiments

Faulty motors are classified into four groups:

- increased friction in brush–commutator contact;
- bearing fault;
- contact between fan and housing;
- howling.

Motors labelled with the ''howling'' attribute produce an unpleasant sound, typically at lower rotational speeds. This sound can be registered during motor rundown. Howling itself is a manifestation of a fault in the rotating parts, more precisely, the final shape of the fan after balancing. It appears intermittently in a relatively short time interval. It takes skill and experience to recognize it, which is not a problem for experienced quality control operators.

4.1. Motor velocity profile

Good fault isolation requires running a motor under a specific velocity profile. It turns out that all faults except howling are detectable from a sound signal recorded at a *constant* rotational speed. This speed has to be low enough to suppress the effects of aerodynamic noise. Given the fact that howling occurs intermittently at different rotational speeds, it is necessary to scan the sound signal recorded across a wide enough range of speeds. Moreover, if a measurement on a particular motor is repeated several times at the same rotational speeds, howling effects can differ quite significantly. Therefore, an entire range of speeds must be checked for clear and reliable detection of this kind of fault.

Fig. 5 shows a velocity profile suitable for diagnostic purposes. Section A represents the central part of the velocity profile. The constant speed is chosen in a way that emphasizes the noise component contributed by mechanical faults vis-à-vis aerodynamic noise. It will be shown in the next section that all faults, except howling, can be detected or even isolated from the noise signal recorded during interval A. Sections B1 and B2 form a unique profile whose purpose is to scan the speed range that is of interest for the detection of howling. The applied time and velocity landmarks are given in Table 1.

The values of time and velocity landmarks were chosen heuristically on the basis of thorough experimentation.

4.2. Tools

For the sake of feature extraction, the following simple signal processing tools have been applied:

- root mean square (RMS) of the sound signal;
- power spectrum density;

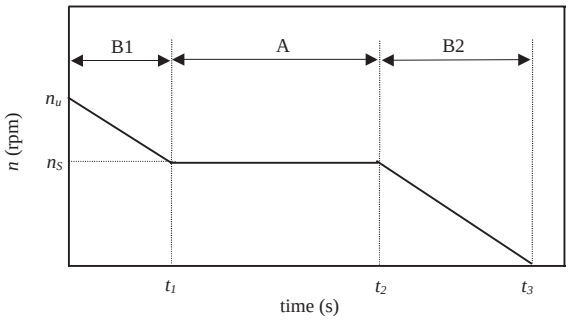

Fig. 5. Rotational speed profile during measurement that enables detection of all faults.

Table 1
Landmarks for the velocity profile

t_1 (s)	t_2 (s)	t_3 (s)	n_u (r.p.m.)	n_s (r.p.m.)
3	8	12	4200	3000

- short-time Fourier transform and
- Hilbert transform.

4.2.1. RMS

The RMS of a signal $x(\Delta t)$ is defined as follows:

$$\mathrm{RMS}(x(k\Delta t)) = \sqrt{\frac{1}{N}\sum\nolimits_{k=0}^{k=N-1} x(k\Delta t)^2}, \tag{2}$$

where Δt is the sampling period, N the number of samples of signal x and $k = 0, \ldots, N-1$.

4.2.2. Power spectrum density (PSD)

The PSD of a signal $x(\Delta t)$ is estimated by means of the periodogram, which reads as follows:

$$\mathrm{PSD} = \frac{1}{N\Delta t}|DFT[x(k\Delta t)]|^2, \tag{3}$$

where $DFT[x(k\Delta t)]$ denotes the discrete Fourier transform of a signal $x(\Delta t)$ defined as

$$X(m) = DFT[x(k\Delta t)] = \Delta t \sum_{k=0}^{N-1} x(k\Delta t)\mathrm{e}^{-\mathrm{j}2\pi(M/n)}. \tag{4}$$

To decrease the variance of the PSD estimate and to prevent leakage,[3] the technique of windowing, window overlapping and averaging were employed. The original signal was windowed using the Hanning window. The length of the window determines the frequency resolution, while

[3] Leakage is the spreading of energy across the frequency spectrum caused by the DFT of the frequencies that are not periodic within the time interval of the signal.

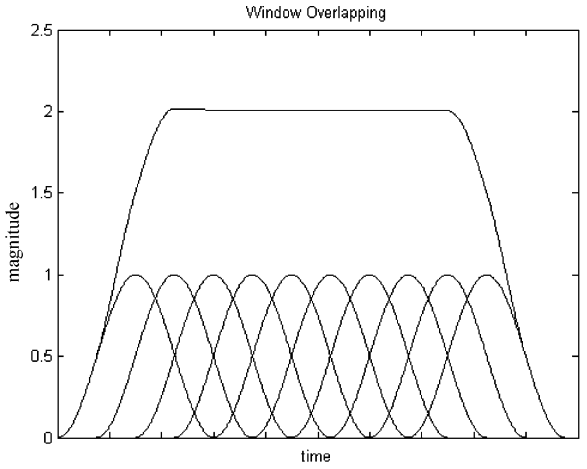

Fig. 6. 75% window overlapping.

the shape of the window is important for preventing leakage. The longer the window, the higher the frequency resolution. If the signal were noise-free, the best choice would be the longest window possible. As physical signals always contain noise, using only one window would result in increased variance of the PSD estimate. To reduce variance, the signal was divided into several segments and the average of the periodograms of these segments was then used as the PSD estimate. To get a higher frequency resolution at low variance, 75% overlapping of the windows (segments) was used (see Fig. 6).

4.2.3. Short-time Fourier transform (STFT)

If the frequency content of a signal varies with time, the signal cannot be treated using the traditional Fourier Transform. Short-time Fourier transform (STFT) was introduced in 1946 by Gabor to provide a time–frequency picture of a signal. Here, the signal $x(t)$ is multiplied with a window $w(t-\tau)$ centred or localized around time τ and the Fourier transform of function $f(t,\tau) = x(t)\cdot w(t-\tau)$ is computed:

$$X(\omega,\tau) = F(f(t,\tau)) = \int_{-\infty}^{+\infty} x(t)w(t-\tau)\mathrm{e}^{-\mathrm{j}\omega t}\,\mathrm{d}t. \tag{5}$$

The sufficient conditions for the existence of transform (5) are as follows [15]:

1. $\int_{-\infty}^{+\infty} |f(t,\tau)|\,\mathrm{d}t$ exists.
2. There are a finite number of discontinuities in $f(t,\tau)$.
3. The function $f(t,\tau)$ has bounded variation. A sufficient weaker condition is fulfillment of the Lipschitz condition.[4]

[4] A function $f(x)$ satisfies the Lipschitz condition of order α at $x=0$ if

$$|f(h)-f(0)| \leqslant B|h|^{\beta}$$

for all $|h|<\varepsilon$, where B and $\beta>0$ are independent of h, and α is an upper bound for all β for which a finite B exists.

In practical cases the discrete version of Eq. (5) is used. STFT is computed only for discrete values of ω and for the finite number of window positions τ. With STFT the time domain is mapped into the time–frequency domain.

4.2.4. Hilbert transform

The Hilbert transform of a signal $x(t)$ is an integral transform defined as [16]

$$\mathrm{H}\{x(t)\} = \tilde{x}(t) = p.v.\frac{1}{\pi}\int_{-\infty}^{+\infty} x(\tau)\frac{1}{(t-\tau)}\,\mathrm{d}\tau = \frac{1}{\pi}x(t) * \frac{1}{t}, \tag{6}$$

where $p\cdot v.$ denotes the Cauchy principal value of the integral [17]. The signal $x(t)$ and its Hilbert transform $\mathrm{H}\{x(t)\}$ yield the analytic signal[5] in the following way:

$$z(t) = x(t) + \mathrm{jH}\{x(t)\} = |z(t)|\mathrm{e}^{\mathrm{j}\phi(t)}. \tag{7}$$

If $x(t)$ is a monocomponent signal[6], the amplitude of an analytic signal $|z(t)|$ represents the instantaneous amplitude or signal envelope while the phase of the signal $\phi(t)$ equals instantaneous phase. Remember that the instantaneous frequency *IF* can be derived from instantaneous phase in the following manner

$$IF(t) = \frac{1}{2\pi}\frac{\mathrm{d}\phi}{\mathrm{d}t}. \tag{8}$$

In the ideal case *IF* is constant and can be referred to as the carrier frequency. It turns out that in this case *IF* can be treated as constant without any loss of information.

The Hilbert Transform can be effectively applied as a demodulation technique. Moreover, if the signal is monocomponent, the transform inherently selects the higher frequency of the signal as the *IF* and the lower frequency as the envelope without prior knowledge about the signal. This renders construction of the signal envelope possible even if the exact value of the carrier frequency is not known. This approach is also utilized in this case, where the carrier frequency varies for different motors.

The interested reader is recommended to refer to the excellent tutorial [16], which provides the details about the Hilbert transform.

5. Features extraction

Although the noise sources are quite well understood, the motor sound displays very unpredictable, unsteady and vicissitudinary behaviour. That is, if the sound of a particular motor is recorded twice under the same conditions, the power spectrum densities of the respective sound signals can differ significantly. Although the same significant frequency components appear in both PSDs, their magnitudes can differ by 300% or even more. This can be explained by two facts. Firstly, small fluctuations in rotational speed imply smearing of the power of speed-dependent components. Instead of a single excited frequency component one usually gets a

[5] Analytic signal is a signal, which satisfies Cauchy–Riemann conditions for complex signals [18].

[6] Monocomponent signal is a signal in which the amplitude of only one frequency component varies as a function of time [16]. In terms of frequency domain, monocomponency means that the spectra of amplitude $|z(t)|$ and phase $\phi(t)$ of a signal are non-overlapping.

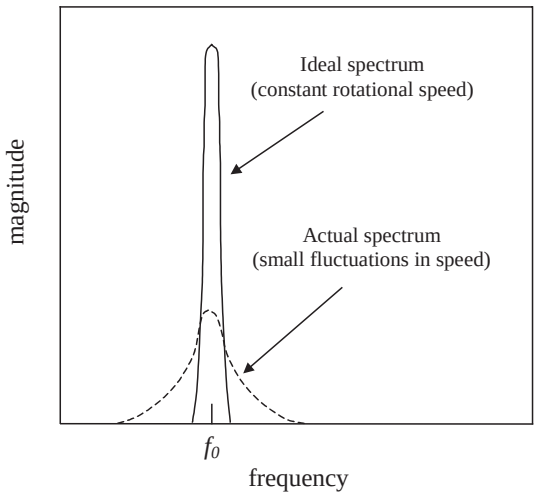

Fig. 7. Influence of small fluctuations in rotational speed on a single component in spectrum.

(narrow) frequency band excited (see Fig. 7). Secondly, sound sources of the motor are not ideally stationary but inherently comprise certain degree of unsteadiness, which results in fluctuating magnitudes of the spectrum. In order to decrease the influence of above phenomena on fault diagnosis, two remedies are applied. Firstly, for the purpose of fault isolation and feature extraction one cannot use absolute values of a single frequency component but should rather take into account narrow bands around this component. Secondly, to diminish the effect of unsteadiness, the signal must be long enough in order to average out the fluctuations.

Fig. 8 depicts two power spectrum densities of sound signals of the *same* motor taken during two consecutive recordings. It clearly shows that even though the recordings were made under the same conditions, the components at characteristic frequencies differ substantially. Due to greater fluctuations in rotational speed, power in case (b) is spread into wider frequency band than in case (a).

5.1. *Fault-free motor*

A fault-free motor is significantly less noisy than a faulty motor. The contributions of mechanical sources are negligible. Electromagnetic noise prevails over all other sources (see Fig. 9). The spectrum is depicted only to the frequency of 3500 Hz because the power contribution of higher frequencies is negligible. The greatest component (100 Hz) belongs to electromagnetic sound (marked Em) and a few smaller peaks (marked Ad) belong to the aerodynamic source (fan impeller). The power of the components in the frequency range around 1000 Hz is increased because the eigenfrequencies of the motor are in this frequency range.

5.2. *Increased friction in brush–commutator contact*

The commutator comprises 22 commutator bars. In every rotor revolution the brush slides over all of them and each impact between brush and commutator bar generates specific noise.

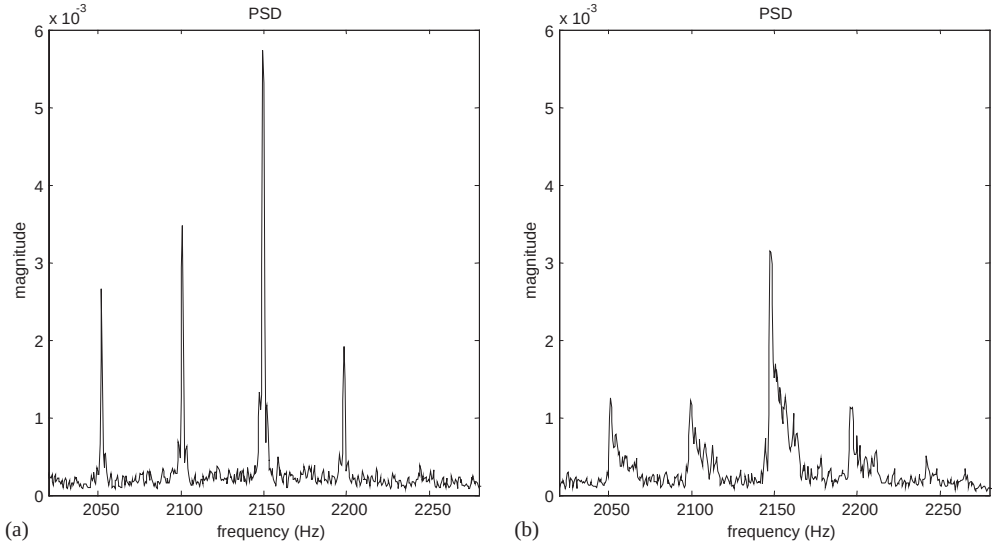

Fig. 8. (a and b): Comparison of PSDs of the same motors taken during two consecutive recordings.

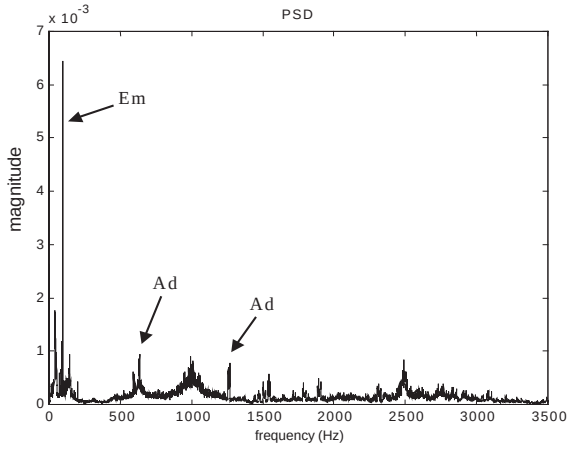

Fig. 9. PSD of a fault-free motor.

Although there are two brushes positioned diametrically on the commutator, they slide over the commutator bars simultaneously so in every rotor revolution 22 impacts can be heard. In the power spectrum this is presented with a peak at frequency

$$f_i = f_r 22i, \quad i = 1, 2, 3 \ldots \tag{9}$$

and its higher harmonics (f_r denotes shaft rotational frequency, i.e., number of rotor revolutions per second, and i denotes higher harmonics).

Malfunction in brush–commutator contact occurs in the case of increased force in the spring that keeps the brush in permanent contact with the commutator. Increased force causes increased

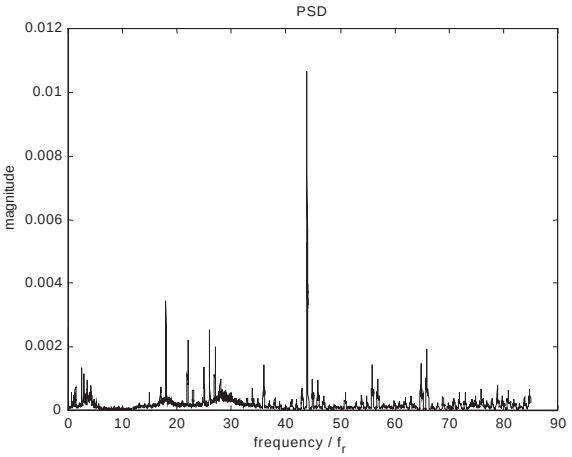

Fig. 10. PSD of a motor with fault in the brush–commutator contact.

friction, and therefore more intense sound. The corresponding spectrum is characterized by increased magnitudes of significant characteristic frequencies (9).

Fig. 10 depicts the PSD of the faulty motor with the corresponding fault. In this case only the magnitude of the second harmonic ($i = 2$) is extremely augmented. Higher harmonics are not presented in the figure because, in comparison with the characteristic frequencies (9), they are negligible.

5.3. *Bearing fault*

In general, the rolling bearing comprises two rings: the outer raceway and the inner raceway. In the space between them they create a special track, which is lubricated and filled with a set of rolling elements (Fig. 11).

In the frequency domain analysis, five vibration frequencies [19,9] are important for detecting the faulty bearing. These frequencies are explained in Table 2.

In this case the number of rolling elements $Z = 7$, and the ball (B) and cage (C) diameters are 4 and 15 mm, respectively.

Each rotating part of a bearing rotates with a different revolution frequency (see Table 2). Consequently, a defect on any of them (raceway, ball) causes repetitive impacts between this and adjacent parts during revolution. These impacts result in recurrent high frequency bursts, i.e., amplitude modulation of sound signal. A burst comprises several different high frequency components, which differ for different motors. The common characteristic of all the motors is that these frequencies usually appear in the following frequency bands:

- 2500–3300 Hz;
- 3500–4000 Hz;
- 4300–4600 Hz;
- 5000–6500 Hz.

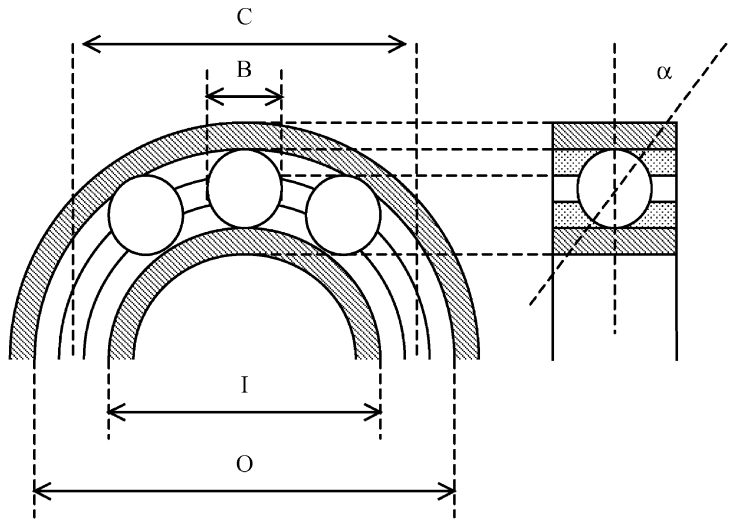

B ball diameter
C cage diameter
I inner race diameter
O outer race diameter
α angle of contact

Fig. 11. Rolling element bearing.

Table 2
Bearing frequencies

Shaft rotational frequency	$f_r = \dfrac{\text{Shaft speed in r.p.m.}}{60}$
Cage rotational frequency	$f_c = \dfrac{f_r}{2}\left(1 - \dfrac{B}{C}\cos\alpha\right)$
Outer raceway frequency	$f_o = \dfrac{f_r}{2} Z\left(1 - \dfrac{B}{C}\cos\alpha\right)$
Inner raceway frequency	$f_I = \dfrac{f_r}{2} Z\left(1 + \dfrac{B}{C}\cos\alpha\right)$
Ball rotational frequency	$f_B = f_r \dfrac{C}{2B}\left[1 - \left(\dfrac{B}{C}\cos\alpha\right)^2\right]$

Modulation frequency equals the revolution frequency of the defective part (Table 2). Experimental results show that the most usual bearing faults that occur in the investigated motor are the ball defect and inner race defect. Using the particular bearing dimensions in expressions given in Table 2, these two faults result in the following modulation

frequencies f_m:

$$\text{Ball defect} \quad f_m = f_r 1.75i, \quad i = 1, 2, \ldots, 5, \tag{10a}$$

$$\text{Inner race defect} \quad f_m = f_r 4.4i \quad i = 1, 2, \ldots, 5 \tag{10b}$$

or very close to these frequencies (i denotes higher harmonics).

In some motors with faulty bearings the power of the sound signal is spread over a wide frequency range, with no clear modulation frequency or idiosyncratic pattern. In this case, it is very difficult to determine the source of the fault because motors labelled with the attribute "impact between fan and housing" share similar characteristics. However, such a motor can still be detected and diagnosed as faulty, but the source of the fault cannot be identified solely from sound analysis.

The next three examples show PSDs typical of bearing faults. The first example illustrates a ball defect. In the second example the location of the fault cannot be allocated to one specific defect. Most likely, this might be due to an improper assembly, which inflicts severe damage upon the bearings. A motor with such a fault is expected to break down within about 30 h of operation (normally, the lifespan is about 700 h). Fortunately, such cases are rather rare. The last example addresses the inner race defect.

The first PSD, depicted in Fig. 12, has one modulation frequency (with higher harmonics) and one carrier frequency component. The modulation frequency follows expression 10a and reads approximately $f_m = 1.75 f_r$. The carrier frequency is 2790 Hz. The estimation is done by means of Eq. (8).

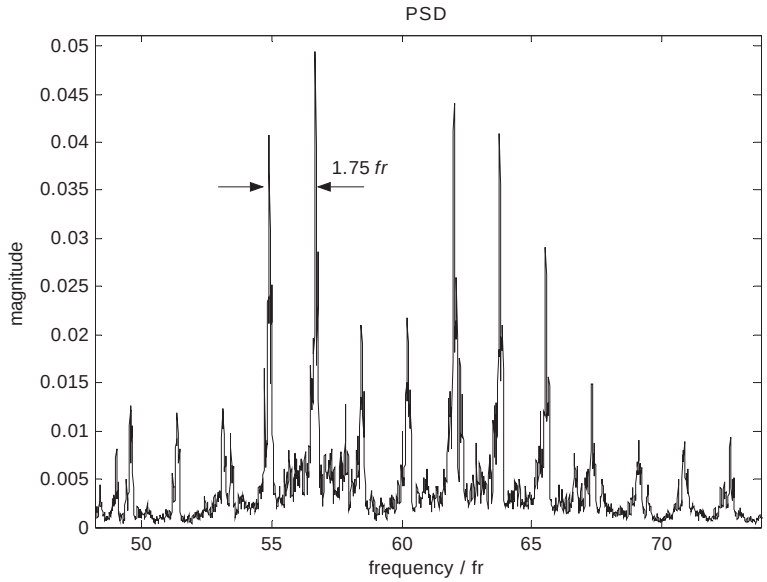

Fig. 12. Example 1: Power spectrum density (frequency is normalized with the rotational speed f_r).

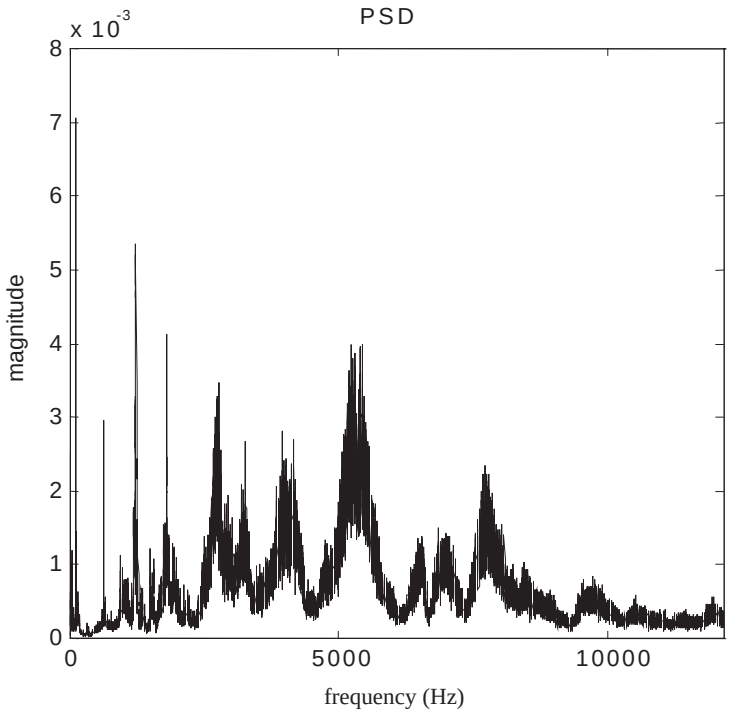

Fig. 13. Example 3: Power spectrum density (frequency is normalized with the rotational speed f_r).

The second typical spectrum is given in Fig. 13. In this case the energy of the sound signal is spread over a wide frequency range (from 3 to 10 kHz) with no clear modulation frequency. The power of this frequency range is rather high in comparison with a fault-free motor.

The third example presents the PSD of an inner race defect. Fig. 14 clearly shows that the modulation frequency f_m is in accordance with Eq. (10b). The carrier frequency of this particular case is 3075 Hz.

Amplitude modulation of the sound signal with a significant modulation frequency (10) is the key feature for a motor with a faulty bearing.

5.4. Howling

Different motors exhibit howling at different rotational speeds; an entire range of speeds must therefore be checked for detection of this kind of fault. According to the velocity profile (see Fig. 5), sections B1 and B2 are useful for this purpose. In order to obtain the frequency content of the sound signal as a function of time, the STFT must be applied. As the STFT is used, the power spectrum likewise becomes a function of time.

Fig. 15 depicts two power spectrum densities. PSD (a) belongs to a fault-free motor, while PSD (b) belongs to a motor labelled with the attribute ''howling''. The difference between sounds generated by these two motors is obvious. The sound of a fault-free motor has increased power of significant frequencies (due to electromagnetism, aerodynamics and brush commutator contact)

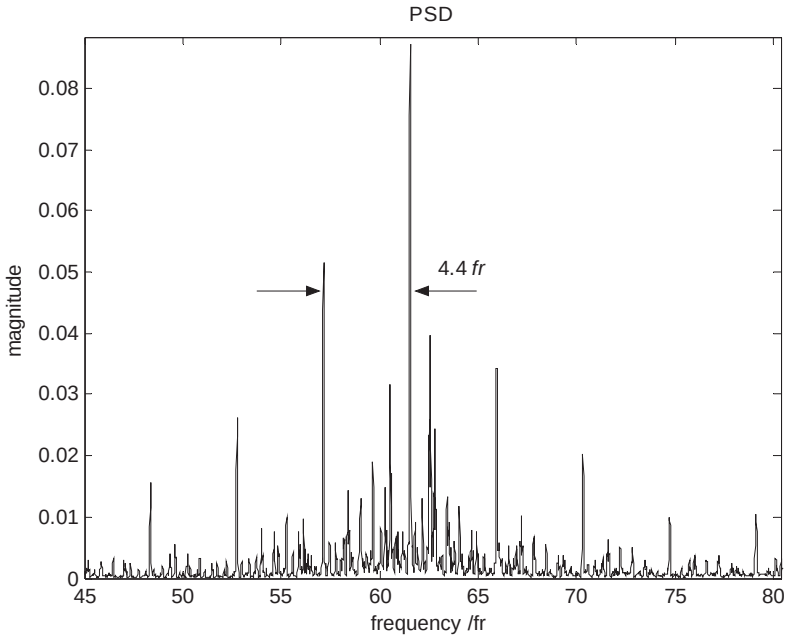

Fig. 14. Example 4: Power spectrum density (frequency is normalized with the rotational speed f_r).

while the "howling" motor has a highly increased power of frequency band between 9 and 13 kHz. Moreover, the power of this frequency band is speed-invariant.

5.5. *Impact between fan and motor housing*

In some motors the fan impeller is incorrectly attached to the shaft. During rotation at low rotational speeds, the fan shimmies and rubs against the motor housing and adjacent parts, which results in the emitted noise. As the rotational speed increases, the airflow through the motor increases along with air pressure at the input airflow port. High air pressure fixes the fan and prevents it from shimmying and therefore from rubbing against the motor housing. Thus, this noise disappears at higher rotational speeds.

In the sound of the motor this contact results in increased power of all frequencies in the frequency range between 3 and 8 kHz (energy is spread over the whole frequency band). The spectrum is similar to the spectrum of the motor with a faulty bearing (see Fig. 14); therefore it is not depicted. In summary, this fault cannot be recognized but can certainly be detected.

6. Diagnostic procedure: fault detection part

The entire diagnostic procedure is presented in Fig. 16. It can be divided into three parts:

- signal acquisition (measurement part, Part 1);
- feature extraction and detection (Part 2 A and B);
- fault localization (Part 3).

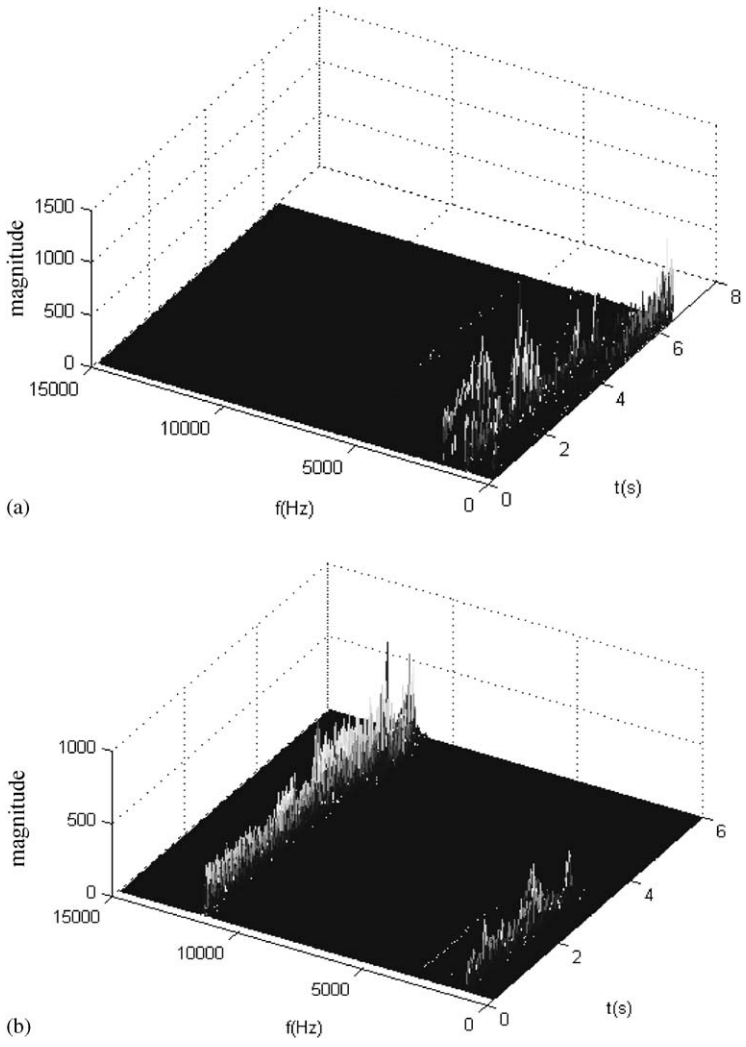

Fig. 15. PSD in the time–frequency domain for a fault-free (a) motor and a motor labelled with the attribute "howling" (b).

The measurement is performed according to the velocity profile presented in Fig. 5. The recorded sound signal then enters Part 2. Part 2-A uses only section A while the right branch uses all sections (B1, A and B2). In addition, the original signal of the left branch is filtered with two bandpass filters (BPF). Three signals, two filtered and the original one (section A), are then used to calculate the RMS. The RMS values of the filtered signals (X_{11}, X_{12}) represent the square root of the signal power of different frequency bands, and the RMS of the original signal (X_2) represents the square root of the power of the entire signal. Therefore, the squared ratios (Y_{11}, Y_{12}) between the RMS of the filtered signals (X_{11} and X_{12}) and the RMS of the original signal (X_2) are the features representing portions of power contributions that belong to the

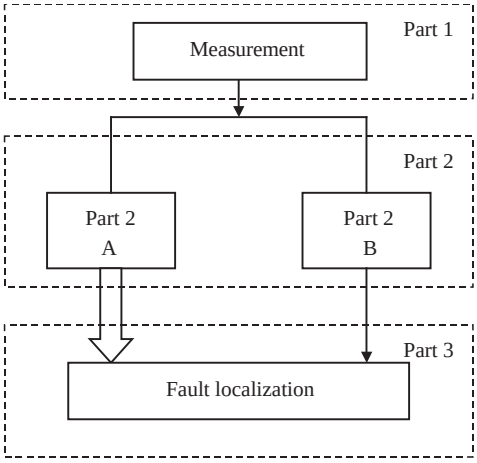

Fig. 16. Diagnostic procedure based on sound analysis.

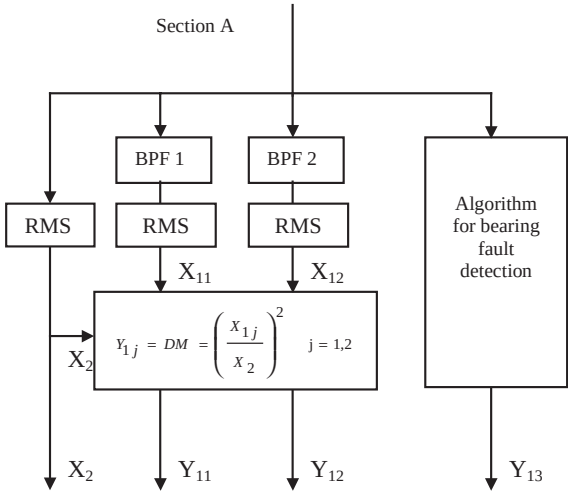

Fig. 17. The structure of part 2-A.

underlying frequency bands. The structure of part 2-A is depicted in Fig. 17. BPF 1 represents the selective bandpass filters which pass the frequencies ($f = 22if_r$, $i = 1,2,\ldots, 10$), and BPF 2 has cut-off frequencies at 3 and 9 kHz.

The RMS of the original signal (X_2) is also a feature useful for fault detection, because faulty motors usually produce more intensive noise than fault-free motors and can therefore already be detected by RMS evaluation with a properly selected threshold value. If the RMS exceeds the threshold value, the motor is considered to be faulty; otherwise it is fault-free. Fig. 18 compares the RMS values of motors with different faults with the RMS of the fault-free motor. Obviously, motors with these faults can be reliably detected only by RMS evaluation.

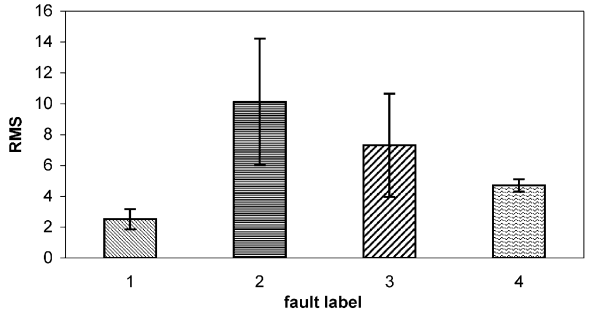

Fig. 18. Comparison of RMS values: fault-free motor (1), increased brush–commutator friction (2), bearing fault (3) and contact fan-housing (4).

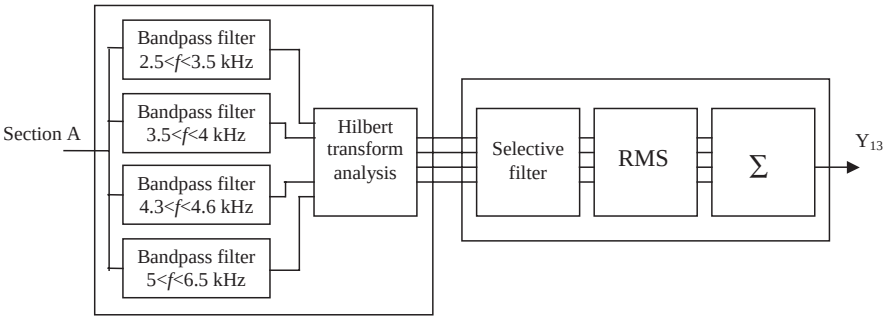

Fig. 19. Procedure for bearing feature extraction.

To recognize a bearing fault, the original signal (section A) is treated with a special signal processing algorithm capable of estimating the power of specific frequencies in the signal envelope. The algorithm comprises two parts (see Fig. 19).

The first part serves to construct the signal envelope. The envelope is obtained by means of Hilbert transform analysis. In order to employ the transform for the purpose of envelope construction, the signal is first refined to isolate the part of the signal excited by a faulty bearing. As a faulty bearing can excite each of four frequency bands (see Section 5.3), i.e., the amplitude modulation can appear in any of them, the signal is first filtered by a set of bandpass filters (Fig. 19). The filtering is needed not only to isolate significant parts of the signal but also to transform the signal into four monocomponent signals, which, unlike the original signal, can have the Hilbert transform analysis readily applied for the purpose of envelope construction. The envelopes are obtained by means of expression (7). In case of a faulty motor, at least one of four envelopes has increased power of the frequencies significant for the bearing fault (10). On the contrary, in motors with flawless bearings, the magnitudes of these frequencies are negligible.

The second part serves to estimate the power of significant frequencies in the envelopes. Here, the envelopes are passed through a selective filter, which removes all frequencies except those germane to different bearing faults (10). Finally, the RMS values of the obtained signals are summed and used as a feature (Y_{13}).

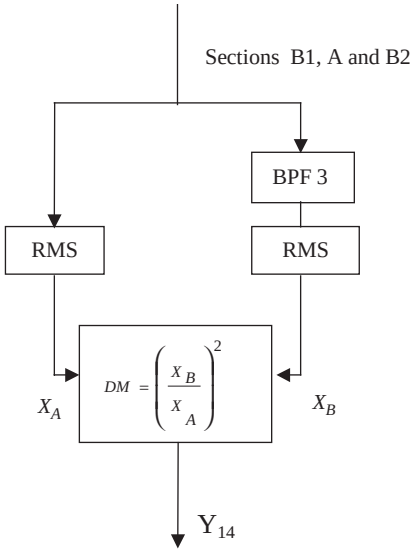

Fig. 20. The structure of part 2-B.

The part 2-B is applied exclusively for the detection of "howling" motors. Two approaches are used. In the first, the RMS of the entire (unfiltered) sound signal is evaluated, while in the second the RMS of a filtered signal (BPF 3 has cut-off frequencies at 9 and 13 kHz) is evaluated. The ratio of filtered and unfiltered RMS values is a feature (Y_{14}) that enables the detection of a "howling" fault. Fig. 20 depicts the structure of part 2-B.

7. Fault localization by means of approximate reasoning

Part 3 of the procedure serves to estimate the location of a fault based on features extracted in Part 2 (Y_{11}, …, Y_{14} and X_2). The result is a list of suspected faults with associated measures of belief, which is a real number between 0 and 1.

7.1. Incidence matrix

The basis for reasoning is the relationship between features (X_2, Y_{11}, …, Y_{14}) and faults (Table 3). Entry "1" in the table indicates that the fault affects the corresponding feature. On the contrary, the value "0" indicates independence between the fault and the related feature.

Fault 1: Brush–commutator contact.
Fault 2: Bearing fault.
Fault 3: Contact between fan and housing.
Fault 4: Howling.

Threshold values for features were chosen heuristically on the basis of quality requirements.

Table 3
Incidence matrix

	Fault 1	Fault 2	Fault 3	Fault 4
X_2	1	1	1	1
Y_{11}	1	0	0	0
Y_{12}	1	1	1	0
Y_{13}	0	1	0	0
Y_{14}	0	0	0	1

7.2. The transferable belief model

In this paper, the Transferable Belief Model (TBM) is adopted [20]. Besides degrees of belief for each fault candidate, the approach also provides a measure for confidence in diagnostic results, referred to as *strength of conflict*.

The TBM derives from the Dempster–Shafer theory of evidence by introducing the concept of 'open-world'. It simply says that the set of all propositions Ω consists of the three subsets: (PP) the set of possible propositions, (IP) impossible propositions and (UP) the unknown propositions. Classical reasoning schemes do not operate with UP.

The purpose of the TBM is to compute the belief masses for the fault candidates $PP = \{f_1, f_2, \ldots, f_K, ff\}$ given the measured features $\{r_1, r_2, \ldots, r_M\}$ [21,22]. Here ff denotes the fault-free case. There is no need to consider elements of IP, as the beliefs are assigned only to PP. Elements of UP can be transferred to PP if new evidence becomes available. The qualitative relationship between faults and residuals is expressed in terms of the incidence matrix $\Lambda = [\lambda_{ij}]$. An entry $\lambda_{i,j} \neq 0$ means that the jth fault triggers the ith feature ($|r_i| \geqslant h_i$). The symbol h_i denotes the predefined threshold value.

TBM reasoning is performed in two steps. In the first step, basic belief masses m are assigned to the subsets $A_i = \left\{ \bigvee_{\lambda_{i,j} \neq 0} f_j \right\}$ and $B_i = \left\{ \bigvee_{\lambda_{i,j}=0} f_j \vee ff \right\}$, $i = 1, 2, \ldots, K$, $j = 1, 2, \ldots, M$, where A_i and B_i are mutually complementary ($m(B_i) = 1 - m(A_i)$).

The belief masses can be set-up as follows:

$$m_i(A_i) = \frac{1}{1 + ((1-a)/a)(h_i/r_i)^{2\gamma}}, \tag{11}$$

where a is the belief mass assigned at threshold h_i and γ is an adjustable smoothing parameter (see Fig. 21).

In the second step, the belief masses $0 \leqslant m(f_i) \leqslant 1$ for individual faults and the fault-free case are calculated by using the unnormalized Dempster rule of combination. In the diagnostic context, where residuals are used as the source of evidence, the rule takes the following form:

$$m(f_i) = (m_1 \oplus m_2 \cdots \oplus m_K)(f_i) = \prod_{\substack{j=1 \\ f_i \in A_i}}^{k} m_j(A_i) \prod_{\substack{j=1 \\ f_i \in B_i}}^{k} m_j(B_i). \tag{12}$$

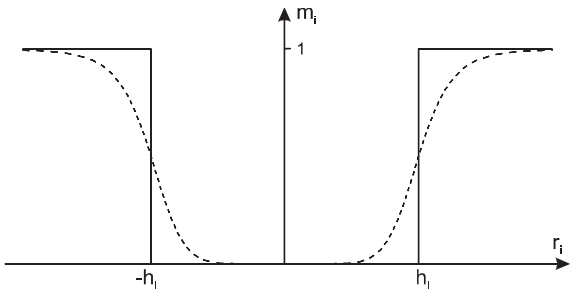

Fig. 21. Basic belief assignment function.

As a result, a ranked list of faults is obtained. Portion of belief not assigned to any of the faulty states is assigned to the empty set:

$$m(\phi) = 1 - \sum_{i=1}^{M+1} m(f_i). \tag{13}$$

This measure is referred to as *strength of conflict*, which may be caused by various sources such as modelling errors, noise and unknown or unforeseen faults. It can be treated as a measure of confidence in the diagnostic results, which provides an interesting feature of this theory.

8. Excerpt from experimental results

As an example of the performance of the diagnostic procedure, three cases are presented as follows: In the first case the motor has Fault 1, i.e., increased friction in brush–commutator contact. As can be seen from Fig. 22, this fault implies increased values of features 1,2 and 3. Since the features are so clear, the localization procedure assigns almost entire belief to the (actual) Fault 1. The *strength of conflict* is almost 0, thus indicating reliable diagnosis.

In the second case the motor has a bearing fault (Fault 2). The relations here are just as clean as in the previous case, which again implies clear reasoning with very low *strength of conflict* (see Fig. 23).

The third case presents a fault-free motor. The motor exhibits slightly increased feature X_2, i.e., the RMS of the entire (unfiltered) acoustic signal. The motor is just a bit louder than average fault-free motors. Fig. 24 shows that the combination of features does not match any combination in Table 3 (only X_2 exceeds the threshold value). Despite this discrepancy, the reasoning still assigns the greatest belief to the fault-free state but with significant *strength of conflict*. In such a case additional inspection or repetition of measurement is recommended.

9. Conclusions

The purpose of the paper is to employ sound analysis in the fault diagnosis of vacuum cleaner motors. The experimental study was conducted on 75 motors. The results show that it is possible to distinguish fault-free motors from those with mechanical faults solely by means of sound

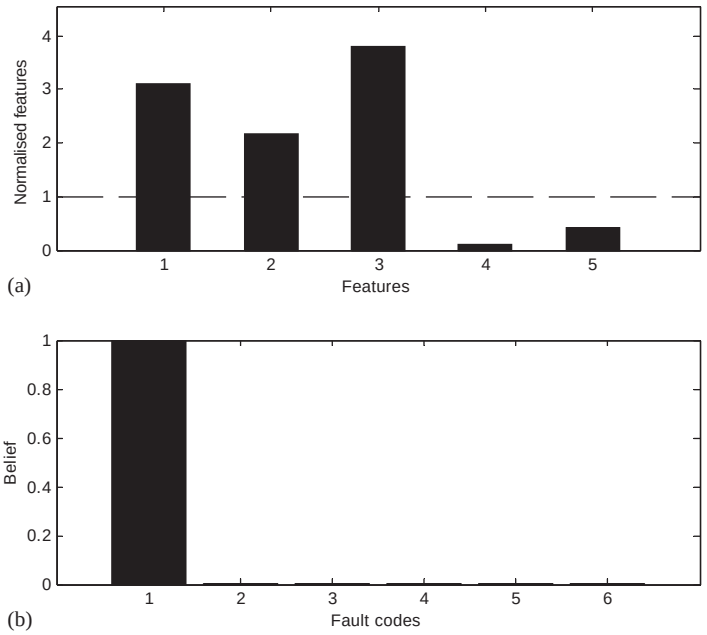

Fig. 22. (a) Normalized features (features divided by corresponding thresholds), (b) reasoning results in case of increased friction in brush–commutator contact (Fault 1); *ff* indicates fault-free and *Sc* indicates strength of conflict.

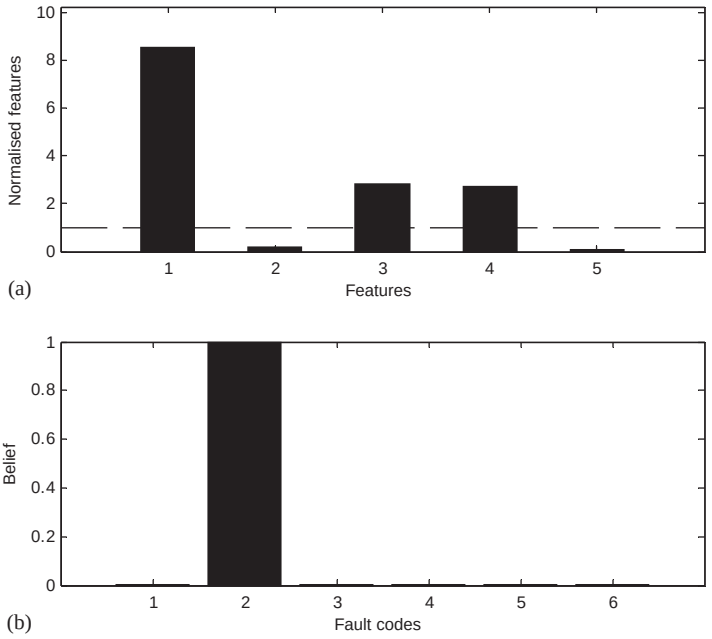

Fig. 23. (a) Normalized features (features divided by corresponding thresholds) and (b) reasoning results in the case of a bearing fault (Fault 2).

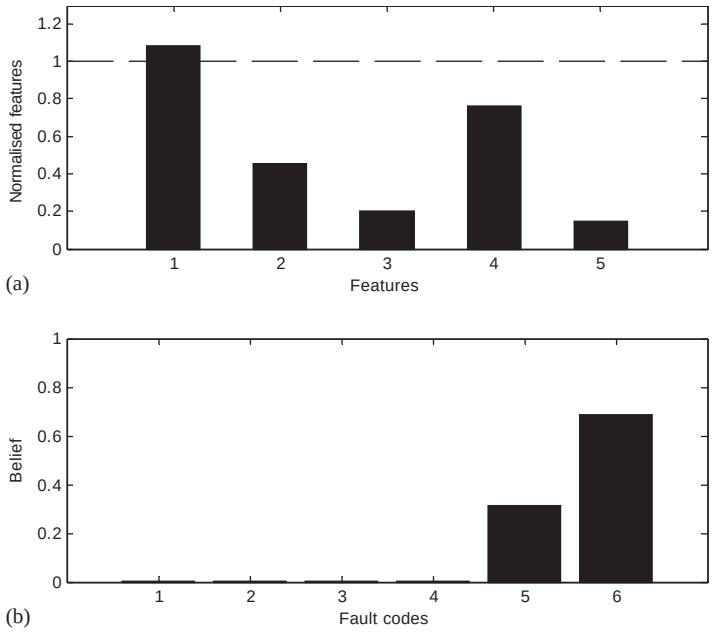

Fig. 24. (a) Normalized features (features divided by corresponding thresholds) and (b) reasoning results in the case of a fault-free motor.

analysis. However, the proposed diagnostic procedure has partly restricted isolation possibilities, i.e., it is able to distinguish three clusters of faults: (increased friction in contact between brush and commutator), (bearing, contact between fan and housing) and (howling). In most cases, it is also able to isolate a bearing fault from the second cluster. It is important to stress that the experiments were carried out under special experimental conditions in an echo-free sound chamber and therefore the proposed diagnostic procedure is in its present form suitable only for laboratory checks, which make up part of the quality assurance process practised by the manufacturer. On-line implementation requires robustness to harsh conditions caused by a noisy environment. For that purpose, further research is in progress, which relies on using several microphones.

Acknowledgements

The authors gratefully acknowledge the support of the company DOMEL and the Slovenian Ministry of Education, Science and Sport.

References

[1] D.M. Yang, J. Penman, Intelligent detection of induction motor bearing faults using current and vibration monitoring, *Proceedings of the 13th International Congress on Condition Monitoring and Diagnostic Engineering Management*, 2000, pp. 461–470.

[2] K. Röpke, D. Filbert, Unsupervised classification of universal motors using modern clustering algorithms, *Proceedings of the SAFEPROCESS 1994*, Espoo, Vol. 2, 1994, pp. 720–725.
[3] D. Filbert, C. Gühmann, Fault diagnosis of electric low-power motors by analysing the current signal, *Proceedings of the SAFEPROCESS 1991*, Baden-Baden, Vol. 1, 1991, pp. 67–72.
[4] D. Filbert, Fault-diagnosis in nonlinear electromechanical systems by continuous-time parameter-estimation, *ISA Transactions* 24 (3) (1985) 23–27.
[5] R. Isermann, Fault-diagnosis of machines via parameter-estimation and knowledge processing—tutorial paper, *Automatica* 29 (4) (1993) 815–835.
[6] Th. Vetter, H. Weber, J. Grossehelweg, Vollautomatische Fehlerdiagnose in der Serienfretigung von Elektromotoren, *VDI-Tagung: Überwachtung und Fehlerdiagnose*, Darmstadt, 1994.
[7] D. Juričić, O. Moseler, A. Rakar, Model-based condition monitoring of an actuator system driven by a brushless dc motor, *Control Engineering Practice* 9 (2001) 545–554.
[8] S. Nandi, H.A. Toliyat, Fault diagnosis of electrical machines—a review, *Proceedings of the IEEE-IEMDC Conference*, Seattle, WA, 1999.
[9] R.B. Randall, State of the art in monitoring rotating machinery, *Proceedings of ISMA 2002*, Vol. 4, 2002, pp. 1457–1477.
[10] A.V. Barkov, N.A. Barkova, The Artificial Intelligence Systems for Machine Condition Monitoring and Diagnostic by Vibration, acquired March 15, 2002, www.vibrotek.com/articles/intelect-eng/index.htm.
[11] Z. Peng, F. Chu, Y. He, Vibration signal analysis and feature extraction based on reassigned wavelet scalogram, *Journal of Sound and Vibration* 253 (5) (2002) 1087–1100.
[12] C. Schenck, Testing and Diagnostic Systems for Vacuum Cleaner Blower, acquired October 5, 2002, www.Schenck.net.
[13] E. Albas, T. Durakbasa, D. Eroglu, Application of a new fault detection technology for quality improvement of appliance motors, acquired November 10, 2002, www.artesis.com/ Products/Mqm/ iatc_2000_artesis_paper.pdf.
[14] R.B. Randall, *Frequency Analysis*, 3rd Edition, Brüel & Kjaer, Copenhagen, 1987.
[15] R.W. Ramirez, *The FFT: Fundamentals and Concepts*, Prentice-Hall, Englewood Cliffs, NJ, 1985.
[16] B. Boashash, Estimating and interpreting the instantaneous frequency—Part 1: fundamentals, *Proceedings of the IEEE* 80 (4) (1992) 520–538.
[17] F.B. Hildebrand, *Advanced Calculus for Engineers*, Prentice-Hall, Englewood cliffs, NJ, 1949.
[18] E. Kreyszig, *Advanced Engineering Mathematics*, 8th Edition, Wiley, New York, 1999.
[19] R. Barron, *Engineering Condition Monitoring, Practice, Methods and Applications*, Longman, New York, 1996.
[20] P. Smets, R. Kennes, The transferable belief model, *Artificial Intelligence* 66 (1994) 191–234.
[21] Y. Peng, P. Arte, R. Hanus, Quantitative model-based fault diagnosis using belief functions, *Prepr. CESA'96 IMACS Multi-Conference*, Lille, Vol. 1, 1996, pp. 528–532.
[22] A. Rakar, Đ. Juričić, P. Ballé, Transferable belief model in fault diagnosis, *Engineering Applications of Artificial Intelligence* 12 (1999) 555–567.